Extreme Mechanics Letters 64 (2023) 102081

Contents lists available at ScienceDirect

Extreme Mechanics Letters

journal homepage: www.elsevier.com/locate/eml

Nano to macro-scale elastic and plastic characteristics of calcium metal and implications for rechargeable battery applications

Jungho Shin [a], Cole D. Fincher [a,b], Matt Pharr [a,*]

[a] Department of Mechanical Engineering, Texas A&M University, College Station, TX, 77840, USA
[b] Department of Mechanical Engineering, Massachusetts Institute of Technology, Cambridge, MA, 02139, USA

ARTICLE INFO

Keywords:
Mechanical testing
Mechanical properties
Nanoindentation
Batteries
Calcium metal
Strength

ABSTRACT

Multivalent metals (Ca, Mg, Al, etc.) are promising for anodes of rechargeable batteries owing to their high theoretical capacity that stems from multiple electron transfer per redox center. Among these multivalent metals, calcium exhibits a low electrochemical potential of −2.87 V (relative to the standard hydrogen electrode) and is the fifth most abundant element in the earth's crust. In addition to resolving electrochemical issues, prior to practical use it remains critical to fully understand calcium's mechanical properties to mitigate any potential degradation and failure mechanisms. To this end, we have conducted mechanical testing of Ca at the nano- and macro-scale through nanoindentation and bulk compression testing. Nanoindentation tests indicate an elastic modulus that ranges from 25.2 to 21.7 GPa and a hardness that ranges from 0.88 to 0.46 GPa as the indentation depth increases from 0.25 to 10 μm. Bulk compression tests show a yield strength of 107 ± 4.6 MPa (average ± standard deviation). These tests demonstrate a minimal sensitivity of calcium's mechanical properties to strain rate or "size effects", which differs from previous studies of alkali metal anodes, likely stemming from Ca's relatively high melting point compared to the alkali metals. We conclude the manuscript by discussing the implications of these measured mechanical properties in the context of energy storage applications.

1. Introduction

Multivalent rechargeable battery systems have been gaining attention to meet the requirements of high energy and power density energy storage systems. Since each multivalent ion can combine with multiple electrons, batteries based on multivalent chemistries can achieve relatively high energy densities [1–7]. Furthermore, multivalent metals (Mg, Al, Ca, Zn) are abundant on earth and are less reactive than alkali metals in ambient air. Among them, calcium metal is promising for battery applications as it is the fifth most abundant element in the earth's crust and has a low standard reduction potential of −2.87 V, which is far lower than that of Mg (−2.37 V), Al (−1.68 V), and Zn (−0.76 V) [8–10]. Additionally, calcium metal anodes have theoretical capacities of 1337 mAh/g and 2073 mAh/cm^3, which are several times larger than graphite-based lithium-ion batteries (372 mAh/g and 800 mAh/cm^3, respectively) [11–14]. Additionally, due to calcium's relatively high stiffness and hardness, calcium-based batteries may find applications as "structural batteries" [15]. Overall, multivalent Ca metal is highly attractive as a potential next-generation energy storage system due to its two-electron redox chemistry, large theoretical capacity, earth abundance, and demonstrated reversible plating/stripping properties [12,16].

During electrochemical cycling, significant stresses can be generated in a battery electrode of varying signs (compression or tension) depending on the loading conditions [17,18]. For example, Zhang et al. reported that compressive stresses on the order of 400–500 MPa during lithiation of a thin film V_2O_5 cathode on a current collecting substrate [19]. Pharr et al. measured a compressive stress of up to 1.2 GPa upon lithiation of a silicon anode [18]. They reported that the lithiated silicon anode flows plastically after a concentration of ~$Li_{0.4}Si$; as such, during delithiation, large tensile stresses develop. In a separate study, Pharr et al. found that compressive stresses of 800–900 MPa developed during lithiation of a germanium anode [20]. Likewise, in calcium-based batteries, compressive stresses have been observed during intercalation into tin [8,9,21]. Large stresses can readily produce nano/micro cracks, which can compromise the overall performance of the battery (e.g., capacity and cyclic performance). Moreover, during plating and stripping, calcium metal undergoes so-called "infinite volume change" [21], which may induce large stresses and plastic deformation. Calcium metal has also been reported to display a lesser propensity to form dendrites

* Correspondence to: Mechanical Engineering Office Building 221, 3123 TAMU, College Station, TX 77843-3123, USA.
E-mail addresses: jungho.shin0912@tamu.edu (J. Shin), cfincher@mit.edu (C.D. Fincher), m-pharr@tamu.edu (M. Pharr).

https://doi.org/10.1016/j.eml.2023.102081
Received 16 June 2023; Received in revised form 28 August 2023; Accepted 15 September 2023
Available online 20 September 2023

than that of lithium and sodium metal [22,23]. However, when calcium does form dendrites, they have been shown to exhibit higher yield strengths than many other metallic dendrites [24,25], e.g., as compared to lithium and sodium [12,26]. Given the relatively high strength of calcium, its dendrites may readily penetrate the (liquid or solid) electrolyte and eventually produce a short circuit in the battery. As such, prior to commercialization, we must gain a detailed understanding of the mechanical properties of calcium metal from the nano to bulk scales as to gain insight into preventing potential degradation mechanisms and safety hazards and increasing cycle life.

Obtaining a detailed knowledge of the mechanical properties of calcium metal in various geometries and under various loading conditions is critical in designing robust batteries. However, surprisingly little is known regarding the mechanical properties of calcium metal, particularly at small length scales [27–29]. Shaw et al. found that Ca metal has yield strength of ∼50–70 MPa and an ultimate tensile strength of ∼70 MPa at room temperature and a yield strength of ∼80 MPa and an ultimate tensile strength of ∼95 MPa at 77 K [29]. However, these measurements are bulk measurements, and most electrochemical deposits of Ca exist at much smaller length scales, e.g., at the nanometer scale in dendritic deposits of Ca. As such, it is important to fully characterize the mechanical properties of Ca at the nanoscale as well. Likewise, it is critical to determine the sensitivity of Ca to loading at various strains rates to assess whether Ca will respond differently when subjected to various loading rates, i.e., different charging rates during electrochemical cycling.

In this paper, we report measurements of the mechanical properties of calcium at the nano, micro, and bulk scales at room temperature. Namely, we measured the nano-scale hardness and elastic modulus of Ca metal through nanoindentation, characterized the micro-scale hardness through micro-hardness testing, and gathered stress–strain data from bulk compression tests performed at different (engineering) strain rates. We conclude the manuscript by discussing the implications of these experimental measurements in the context of battery applications.

2. Materials and methods

2.1. Sample preparation

Calcium shot was purchased from Alfa Aesar with purity of 99% (product number: 10126). The condition of as-purchased Ca metal is unsuitable for mechanical testing due to its irregular shape. As such, the samples were carefully polished with sandpaper under mineral oil (Sonneborn PD-28) and were shaped into rectangular parallelepipeds with widths, lengths, and heights of approximately 0.5 cm × 0.5 cm × 1 cm for bulk compression testing. The dimensions of each sample were measured with calipers, and an average from multiple measurements was taken as the representative dimension. For nanoindentation, Ca samples were embedded in epoxy and then ground and polished using a sequence of 9 μm, 3 μm, and 1 μm steps. To prevent undesired chemical reactions in air, the samples were periodically quenched in liquid nitrogen and polished while still cold. Once the polishing was complete, they were transferred to a DC sputter coater and a protective layer of gold, approximately 10 nm in thickness, was deposited on the polished surface. To measure the grain size, the Ca sample was polished carefully under mineral oil, and the surface was imaged by optical microscope with polarized light (Olympus, DXS 500, RRID:SCR_022202).

2.2. Bulk compression testing

For bulk compression tests, Ca samples were shaped into rectangular parallelepiped (∼0.5 cm × 0.5 cm × 1 cm) by polishing under mineral oil, as described in the previous section. Likewise, specimens for nanoindentation testing had a height-to-width ratio of ∼2.0. Then, the sample was loaded into the mechanical testing system (Instron 3367, 2530 static load cell ± 10 kN). Bulk compression tests were conducted with mineral oil applied to the sample surface to mitigate the effects of chemical reactions with air and to prevent barreling by reducing friction between the sample and the compression platens. Three different strain rates of 0.1, 0.01, and 0.001 1/s were used for compression testing, and the experiments were stopped when the strain reached ∼30%. We note that the strain rates imposed in bulk compression testing are engineering strain rates. The testing results were collected at 50 Hz. Immediately after testing, no changes in color of the sample were observed (thus suggesting minimal surface contamination during testing), and we did not observe any significant effects of barreling.

2.3. Microhardness testing

The Ca samples were embedded in epoxy resin (Buehler, EpoxiCure 2) and carefully polished in mineral oil to prevent undesirable chemical reactions in air. After polishing, petroleum jelly was applied to the surface of the sample to further mitigate any potential effects from air exposure during the microhardness testing. Microhardness testing (Phase II, 900–390 Series) was performed with a Vickers tip at maximum load of 1.96 N, 2.94 N, 4.9 N, and 9.8 N with a dwell time of 10 s at the maximum load. Optical microscope images were taken to measure the contact area of the indents. ImageJ (National Institutes of Health) software was used to estimate the projected contact area, and the presented microhardness (H) was calculated as $H = P/A_{projected}$, where P is load and $A_{projected}$ is the projected contact area (normal to the load). All microhardness tests were conducted in air at room temperature. Immediately after testing, no change in the color of the sample was observed, thus suggesting minimal surface contamination during testing.

2.4. Nanoindentation

Prior to nanoindentation testing, the Ca samples were thoroughly polished (as mentioned in Sample Preparation section above), and a 10 nm protective layer of gold was deposited onto each sample to mitigate undesirable chemical reactions during the tests. Immediately thereafter, nanoindentation experiments (KLA iMicro nanoindentation system with InForce 1000) were carried out to measure the hardness, H, and elastic modulus, E, at room temperature. The continuous stiffness measurement mode (CSM) was used with a Berkovich tip for nanoindentation. Nanoindentation depths ranging from 30 nm to 10 μm were implemented at a constant $\dot{p}/p = 0.05$ (1/s), and the elastic modulus and hardness were determined by the Oliver–Pharr method [30]. Frame stiffness and area function calibration was conducted with fused silica. The dynamic phase angles were corrected based on Hay and Herbert's model to eliminate contributions from the measurement system itself. The parameters for the indenter column – stiffness, damping, and mass – were provided by KLA [31,32]. According to previous studies, in case of CSM test mode, a high dynamic phase angle may occur from details of the dynamics of the actuator and/or plasticity error of the test specimen [33,34]. Large dynamic phase angles (of nominally, >10°) indicate the potential for error in the estimated stiffness — and as a result, we only present modulus and hardness measurements when the corresponding corrected dynamic phase angle is smaller than 10° [33].

3. Results

The shape of the as-received calcium metal was irregular and possesses significant surface roughness. To address this issue, the as-received calcium was carefully polished using sandpaper under oil to produce rectangular parallelepipeds with widths, lengths, and heights of approximately 0.5 cm × 0.5 cm × 1 cm. Additional sample preparation and testing methods are provided in the Experimental Section. Optical imaging of polished Ca specimens provided an estimate of the grain size as approximately 10–40 μm.

Table 1
Mechanical properties of Ca metal reported from various references.

References	Elastic modulus (GPa)	Yield strength (MPa)	Temperature (K)
Our data	21.7 ± 2.7 −25.2 ± 0.43	107 ± 4.6	RT (room temperature)
Shaw et al. [35]	–	48.7 & 81.2	295 & 77
Hampel et al. [36]	–	84.8	RT
Compare Metals (Online Source) [37]	20	–	Not reported (likely RT)
AZO Materials (Online Source) [38]	23.4	–	Not report (likely RT)

3.1. Elastic modulus

Fig. 1 shows the elastic modulus versus indention depth measured from nanoindentation experiments. The average of seven tests are presented, and the error bars indicate one standard deviation from the mean. We note that nanoindentation of calcium metal was conducted within one hour after sample preparation. In the continuous stiffness measurement mode (CSM) of nanoindentation measurements, the dynamic phase angle refers to a phase lag between the applied oscillatory load and the resulting oscillatory displacement of the sample, which can provide insights into the viscoelastic (or viscoplastic) behavior of the material. In Figure S2, the measured and corrected dynamic phase angle are presented, and the measured dynamic phase angle is found to be slightly larger than the corrected dynamic phase angle at a given depth. This discrepancy arises because the raw measured dynamic phase angle has contributions from not only the test specimen but also from that of the measurement system itself. To remove artifacts from the test measurement system itself, we computed the dynamic phase angles based on Hay and Herbert's model. The corrected dynamic phase angle (Figure S2b) becomes constant (flattens out) as the indentation depth becomes larger than ∼ 0.25 μm. Furthermore, the data accuracy of CSM mode relies on the various factors — i.e., instrument factors, such as the physics of the force actuator and displacement measurement, as well as plasticity errors of the test specimen. At the nanoindentation depths <1 μm, the dynamic phase angles reported here as >10° are most likely related to the dynamics of the actuator [31–33]. Additionally, Merle et al. reported that, for materials with a high E/H ratio, a high dynamic phase angle (∼10° or higher) may reflect so-called "plasticity errors" in the dynamic displacement oscillation when it is used for continuous stiffness measurements [34]. In this sense, we note that the corrected dynamic phase angle of Ca metal becomes less than 10° at depths larger than ∼ 0.25 μm. Furthermore, given that a key factor that can induce plasticity error is related to the velocity in relation to the drive frequency (here 220 Hz) and oscillation, we also present the loading rate (dimensionally, $\dot{p}/p$) and the dynamic displacement with respect to depth in Figure S3. For comparative purposes, we have also included data from literature in Table 1. In terms of the elastic modulus, reference 37 (Compare Metals) [37] reports 20 GPa and reference 38 (AZO Materials) [38] reports 23.4 GPa for the modulus of Ca metal.

3.2. Nanoindentation hardness

Fig. 2 shows the nanoindentation hardness of Ca metal as a function of indentation depth. The plot shows an average of seven tests, and the error bars span one standard deviation from the mean. Individual indentation tests were implemented at various (random) positions on the sample surface, and each indentation was sufficiently spaced (much more that the diameter of the indents) to eliminate both its history dependency and any potential plastic zone effects from nearby indentations.

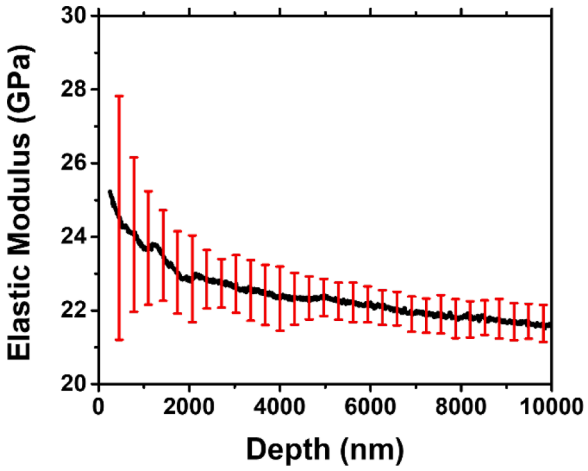

Fig. 1. Nanoindentation test results of the elastic modulus as a function of depth in Ca metal at room temperature. The tests were performed with a constant $\dot{p}/p = 0.05$ (1/s) to a depth of 10 μm. The data (black line) represents the average of seven individual indents, and the error bars (in red) indicate one standard variation from the average. We note that the region where the corrected dynamic phase angle is larger than 10° represents one in which large "plasticity errors" occurred; as such, we have omitted data below ∼ 0.25 μm in reporting the elastic modulus. The individual nanoindentation curves can be found in the Supporting Information Figure S1(a).

A slight decrease in hardness with depth is found up to a depth of ∼ 5 μm, and the hardness remains nearly constant at larger depths. Previous studies on lithium and sodium metal report significant decreases in hardness with nanoindentation depth by more than a factor of ∼6 for lithium and more that a factor of ∼12 for sodium metal across a similar depth range as reported here [39,40]. Here, the nanoindentation hardness of calcium decreases from approximately 0.88 GPa to 0.48 GPa in depths spanning from 250 nm to 10 μm. We should note that a 10-nm layer of gold was deposited on these samples prior to nanoindentation to help mitigate potential effects of surface contamination (e.g., due to chemical reactions with the surrounding environment) affecting our measured mechanical properties during nanoindentation.

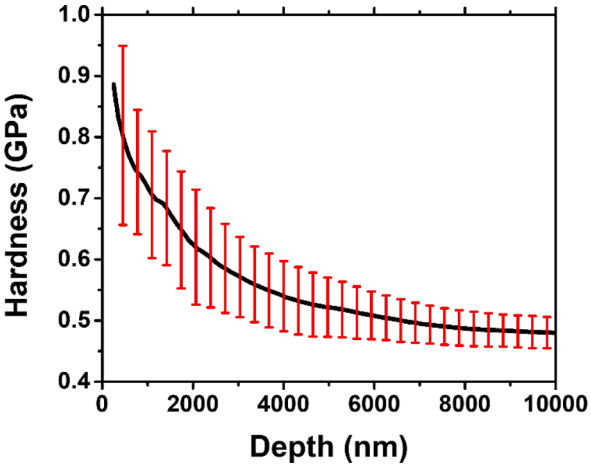

Fig. 2. The measured nanoindentation hardness of calcium metal at room temperature. The data (black line) represents the average of seven individual indents, and the error bars (in red) indicate one standard variation from the average. We note that the region where the dynamic corrected phase angle is larger than 10° represents one in which large "plasticity errors" occurred; as such, we have omitted data below ∼ 0.25 μm in reporting the hardness here. The individual nanoindentation curves can be found in the Supporting Information Figure S1(b). (For interpretation of the references to color in this figure legend, the reader is referred to the web version of this article.)

Despite this protective layer, we did observe a slight change in color of the sample after nanoindentation. However, the hardness approaches a constant value with depth; as such, the influence of any potential surface film likely has little effect on our reported hardness data, particularly at larger indentation depths. Likewise, the nanoindentation elastic modulus decreases from ∼25.2 GPa and gradually approaches a nearly constant value of 21.7 GPa (the values differ by only ∼13% over the depth range from 250 nm to 10 μm). We should note that the elastic modulus is most likely to be determined by atomic bonding, and it is unlikely to be affected by the length scale (i.e., it is unlikely to have a "size effect"). However, the nanoindentation modulus appears to be slightly higher than expected at small depths, perhaps due to the presence of thin surface film during the nanoindentation. Still, as the depth increases, these potential contributions diminish, and the modulus approaches a constant value, again suggesting that the effects of surface contamination on our reported values are likely minimal.

3.3. Microhardness testing

Microhardness testing was performed with a Vickers diamond indenter five times at each load with a dwell time of 10 s as shown in Fig. 3. The microhardness (H) at loads of 1.96 N, 2.94 N, 4.9 N, and 9.8 N were 370.6 ± 30.3 MPa, 364.1 ± 14.6 MPa, 368.4 ± 15.0 MPa, and 338.2 ± 18.1 MPa (average ± standard deviation), respectively. Assuming that the indenter area function is ideal, the corresponding indentation depths would be 14.7 ± 0.7 μm, 18.2 ± 0.4 μm, 23.3 ± 0.7 μm, and 34.4 ± 1.3 μm, respectively.

3.4. Bulk compression tests

Fig. 4 shows engineering stress–strain curves for compression of calcium metal. The stresses were measured at various strain rates of 10^{-2}, 10^{-3}, and 10^{-4} /s; at a strain of 0.08, the measured flow stresses were 112.0 MPa, 103.1 MPa, and 106.1 MPa, respectively. Note that here we use strain values of 0.08 for comparison, as per the Tabor relation: under uniaxial loading, the stress at a strain of 0.08 has been found to correlate well with the measured (nanoindentation and micro-) hardness as $\sigma_f(\varepsilon_p = 0.08) \approx H/3$. The Tabor model was used to relate nanoindentation and microhardness measurements to bulk compression test results (see the Discussion section). Although some fluctuations occur at the lower values of strain (likely due to the slight misalignment of the sample relative to the compression platen), the stress increases quite linearly when the strain is larger than 0.07. We observe no significant strain rate dependence.

4. Discussion

4.1. Elastic properties of Ca metal

A few experimental studies have been conducted to assess the elastic properties of Ca metal, which are presented in Table 1. Shaw et al. measured mechanical properties of Ca metal under tension at room temperature and at 77 K [35]. Mechanical properties of Ca have been reported by Everts and Bagley [41] as well as Hampel and Kolodney [36], but those were limited to calcium samples of relatively low purity (Everts and Bagley did not report the purity, and Hampel and Kolodney used 94%–96% pure Ca metal). Additionally, we have found a few

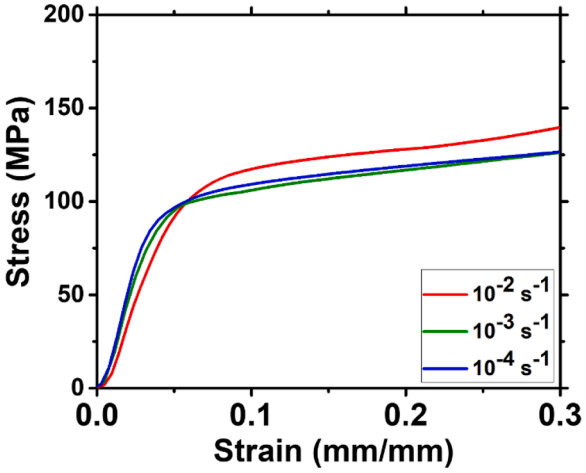

Fig. 4. Engineering stress–strain curves for bulk Ca metal under compression at room temperature. Three tests were conducted at each strain rate, and the averages of each strain rate are shown in the plot. The different colored lines indicate different strain rates: red for 10^{-2} 1/s, green for 10^{-3} 1/s, and blue for 10^{-4} 1/s. The individual curves at each strain rate can be found in the Supporting Information Figure S4.

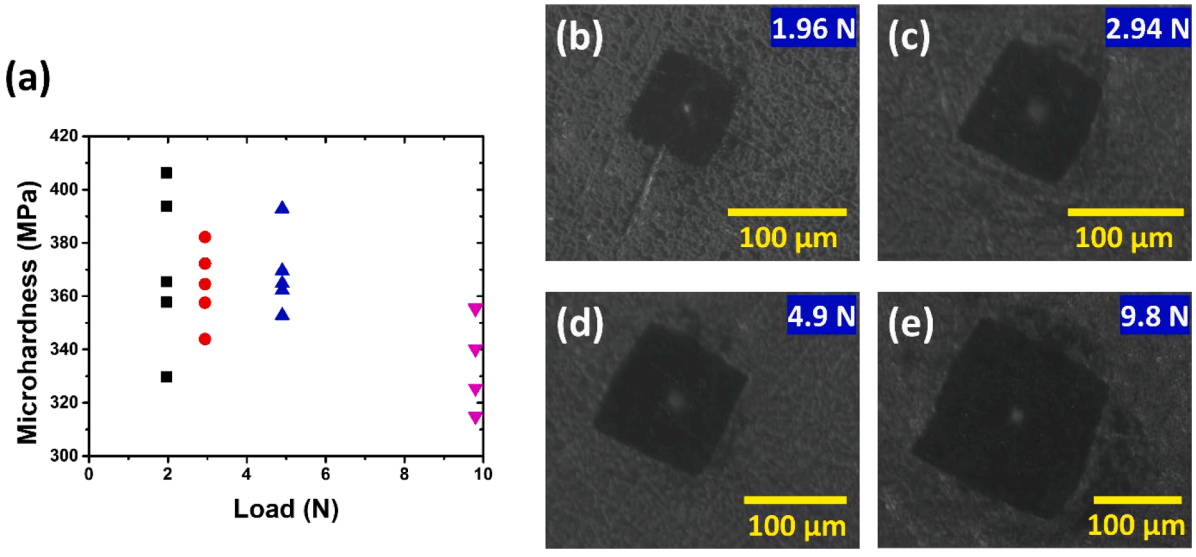

Fig. 3. (a) Microhardness values at different indentation loads. (b)–(e) Optical microscope images of indents at loads of (b) 1.96 N, (c) 2.94 N, (d) 4.9 N, and (e) 9.8 N. Microhardness testing was conducted at room temperature under mineral oil, with a dwell time of 10 s.

online databases of the mechanical properties of Ca, e.g., for Compare Metals [37] and AZO Materials [38], but information related to their measurement methods was not included. Our nanoindentation studies demonstrate an elastic modulus of ~21.7–25.2 GPa, which is indeed comparable to previous studies (Table 1).

4.2. Plastic properties of Ca metal

In Fig. 2, the hardness of Ca metal varies by less than a factor of two over the range of indentation depths (the hardness is 0.88 GPa at a depth of 250 nm, and the hardness is 0.48 GPa at a depth of 10 μm). Furthermore, the microhardness of Ca metal was found to be 0.33 GPa on average (over all tested samples), as indicated in Fig. 3. Although Ca seems to exhibit a slight size dependence of its hardness (varies by a factor of 1.8 over indentation depths from 250 nm to 10 μm), this dependence is relatively small as compared to Na and Li, whose hardness varies by a factor of approximately 12 and 6, respectively, as the indentation depth increase from 250 nm to 10 μm.

The different size dependency (so-called "indentation size effect") of Li, Na, and Ca can be rationalized by considering microstructural details. From a microscopic perspective, dislocations may be lacking at very small scales and result in a "dislocation starvation state", which would thus require a higher stress to cause the metal to flow. Indeed, the dislocation density [42] ρ can be *estimated* by knowledge of the Burgers vector b, shear modulus G, and steady-state flow stress σ_{ss}: $\rho = (\sigma_{ss}/Gb)^2$. We should note that this relation may not be strictly applicable to Ca metal because it is generally accepted for metals that undergo steady-state power-law creep [42,43]. However, even if steady-state power-law creep is not likely to be dominant deformation mechanism for Ca metal at room temperature (due to its relatively high melting point), we still utilize this relation *for estimation purposes* for Ca since steady-state flow stresses in metals are on the same order as their yield strengths [44]. For instance, the steady-state flow stress is typically only a few times less than the yield strength, e.g., a factor of ~3 for Cu, a factor of ~5 for Fe, a factor of ~5 for bronze, a factor of ~2 for stainless steel, etc. [45,46]. For an isotropic material, the shear modulus G can be related to elastic modulus E: $G = \frac{E}{2(1+\nu)}$, where ν is Poisson's ratio. Although Poisson's ratio of Ca has not measured in this study, we take 0.3 as a representative value for a metal. The Burgers vector b is taken as 0.394 nm (for FCC calcium metal whose unit cell length is 558.8 pm); the elastic modulus is taken as 25.2 GPa as measured here; and σ_{ss} is the steady-state flow stress is estimated as the yield strength of Ca measured here, which is 107 MPa (the average in our tests with strain rates ranging from 10^{-2} to 10^{-4} s^{-1}). With these values, the dislocation density of Ca can thus be estimated as 8.5×10^{14} m^{-2}. By comparison, the dislocation densities of Li and Na can be estimated as 2.7×10^{11} m^{-2} and 3.2×10^{10} m^{-2}, respectively (values for these calculations can be found in Table S1). If the dislocations are distributed relatively uniformly through the sample, the average distance (d) between them is on the order of the square root of the reciprocal of the dislocation density [47], $d = \sqrt{1/\rho}$. Through this approximation, the corresponding dislocation spacing (d) in Ca is estimated as ~30 nm, whereas for Li and Na, it is much larger with values of ~2 μm and ~3 μm, respectively. The estimated dislocation spacings in Li and Na are thus larger by a factor of 50 than that of Ca! We note that these dislocation spacings for Li, Na, and Ca metals represent *rough estimations* for comparative purposes rather than precise values.

Still, we should note that we do observe a slight size effect. Although this effect is not very substantial (e.g., as compared to such size effects that have been observed in Li and Na metal), it is still interesting as to hypothesize to its origin. One hypothesis is that the observed size effect may stem from the presence of other inhomogeneities within the Ca metal, such as grain boundaries, voids, and impurities. Namely, when the indentation depth (referred to here as the "length scale") is comparable to the representative size of these inhomogeneities (e.g., the grain size), the mechanical properties will in part reflect the characteristics of these inhomogeneities rather than those of the bulk material. For instance, here we have reported the grain size of the Ca sample as around 10–40 μm. Although these reported grain sizes are slightly larger than the range of the studied nanoindentation depths, it is important to note that the representative size of deformed zone under the indenter is typically several times larger than the indentation depth itself. As such, it is possible that the presence of grain boundaries at large indentation depths (and lack thereof at small indentation depths) contributes to the observed mechanical response during indentation and thus could produce some apparent size effects in Ca. In addition, apart from size effects originating from the material itself, the presence of an imperfect (rounded) indenter tip could lead to an overestimation of hardness, which may result in data that looks like a "size effect". Nonetheless, our estimation of the dislocation spacing provides insight into a likely microstructural explanation as to why Ca exhibits a relatively limited "size effect" as compared to Li and Na.

To connect these values to nanoindentation testing, it is instructive to compare the size of the highly deformed region during the indentation process to the representative dislocation spacing. When the size of the highly deformed region created under an indent (i.e., the plastic zone size) is smaller than the dislocation spacing, on average no dislocations will be involved (activated) in the deformation process. However, if the highly deformed region created under an indent (i.e., the plastic zone size) is much larger the dislocation spacing, numerous dislocations will be involved in the deformation process, and we would expect that the mechanical behavior would approach that of a bulk-sized sample [48]. We note here that the size of this highly deformed region (plastic zone size) during indentation is on the order of (a few times) the indentation depth [39,40]. As such, we suspect that during nanoindentation of Ca, even at relatively small depths (100 nm or so), numerous dislocations are activated and thus contribute to its measured mechanical behavior. By contrast, at small indentation depths (on the order of 100 nm or so), very few or even no dislocations may be activated during nanoindentation of Li and Na, due to the relatively large dislocation spacing estimated in these materials. However, at larger depths (on the order of 1 μm or so), dislocations can indeed be activated during nanoindentation of Li and Na. Upon activation of these dislocations, the strength of Li and Na will be reduced (a lower stress is required to move dislocations), leading to a pronounced size effect, i.e., a reduction in strength with increasing nanoindentation depth. Overall, this analysis provides insight into the microstructural reasons as to why calcium metal exhibits a minimal size effect compared to that of lithium and sodium metal.

From Fig. 4, the strain-stress curves of Ca appear to be insensitive to the strain rate. Previous studies have reported that both lithium and sodium have a significant strain rate dependence of the strength under bulk testing, with strain-rate sensitivity exponents of $m = 0.15$ and 0.2 for lithium and sodium, respectively (to the relationship $\sigma = \kappa\dot{\varepsilon}^m$, where σ is flow stress, $\dot{\varepsilon}$ is strain rate, m is strain-rate sensitivity exponent, and K is a constant) [39,40]. However, calcium metal is nearly insensitive to the applied strain rate at room temperature, i.e., the strain-rate sensitivity exponent at room temperature is approximately 0. This discrepancy is primarily due to the relatively high melting point of Ca (842 °C) as compared to Li (180 °C) and Na (98 °C); the corresponding homologous temperatures at room temperature (T/T_m) are 0.27 for Ca, 0.65 for Li, and 0.8 for Na. At high homologous temperatures, materials tend to exhibit prevalent creep-type behavior. For instance, in Li and Na, power-law creep appears to be readily activated at room temperature and tends to be a dominant mechanism for the deformation [39,40]. However, creep (of any type) is not likely to be dominant deformation mechanism for Ca due to its low homologous temperature at room temperature.

To compare our measured bulk properties to our measured nanoindentation and microhardness results, we take the Tabor relation

$(\sigma_f(\text{at}\quad \varepsilon_p = 0.08) = H/3)$, as to determine whether similar properties are observed at the bulk scale and nanoscale [49]. We compare the flow stress at the strain of 8% ($\varepsilon_p = 0.08$) from the bulk testing and H/3 (a third of hardness) from microhardness and nanoindentation (at 10 μm). As shown in Fig. 5, although H/3 from nanoindentation testing does not exactly equal the measured bulk compressive yield strength, it is in a similar range. Upon closer examination, H/3 from nanoindentation and microhardness testing at similar length scales (i.e., at 10^4 nm) lie within a similar range, albeit with a variation of ~23%. This variation could stem from several factors, including the involved different indentation depths (10 μm for nanoindentation vs. 14.7 μm for microhardness testing), the different geometries of the indenter tips (Berkovich for nanoindentation vs. Vickers for microhardness), slight disparities in data processing methodologies employed, etc. We also note that the hardness measured from microhardness testing is quite similar to that of bulk testing.

4.3. Implications for battery applications

Compared with monovalent metals, multivalent metals such as calcium (Ca^{2+}), magnesium (Mg^{2+}), and aluminum (Al^{3+}), have an intrinsic advantage in theoretical capacity by having multiple electron transfer per redox center. Of these multivalent metals, metallic calcium stands out a promising anode material owing to its relatively low standard potential of −2.87 V, large theoretical capacity of 1337 mAh/g and 2072 mAh/cm^3, and its relative abundance in the earth's crust (5th most abundant element in the Earth's crust) [12]. Additionally, since calcium can form alloys with several other materials, the selection of electrode materials could in principle be quite diverse [26]. For instance, Ca can form several intermediate compounds with Sn, Zn, and Li to Ca_2Sn [50], Ca_3Zn [51] and $CaLi_2$ [52], respectively. Finally, along with Ca^{2+} ions having a smaller polarization strength than multivalent Mg^{2+} and Al^{3+} ions (10.4 for Ca^{2+} vs 14.7 for Mg^{2+} and 24 for Al^{3+}), Ca ions typically have higher mobility than that of magnesium and aluminum, which has key implications in the kinetics (rate) of electrochemical reactions in battery systems [53,54].

In terms of mechanical properties, compared to Li and Na metal, which are well-known anode materials of rechargeable batteries, Ca metal exhibits a much higher yield strength; here we identified an average yield strength of 107 ± 4.6 MPa (in our tests with strain rates ranging from 10^{-2} to 10^{-4} s^{-1}). Indeed, lithium and sodium are very soft and demonstrate extremely low yield strengths; at room temperature, the yield strength of Li has been reported as 0.57 to 1.26 MPa for strain rates from 5×10^{-4} s^{-1} to 5×10^{-1} s^{-1} and that of Na has been reported as 0.15 to 0.29 MPa for strain rates from 10^{-2} to 10^{-1} s^{-1} [39,40]. This soft nature of Li and Na provides some benefits. For instance, for applications in all-solid-state batteries, facile flow provides a potential advantage in maintaining interfacial contact, aka "interfacial wettability". Namely, when external pressure is applied to a battery stack, Li and Na can readily deform and flow owing to their soft nature, which can "fill in" voids at interfaces between the solid electrolyte and the metallic anode, thereby reducing electrical (contact) resistance [55–59]. However, since calcium demonstrates a relatively much larger yield/flow stress, it likely will not provide this advantage of being easily deformed to maintain interfacial contact with a solid electrolyte.

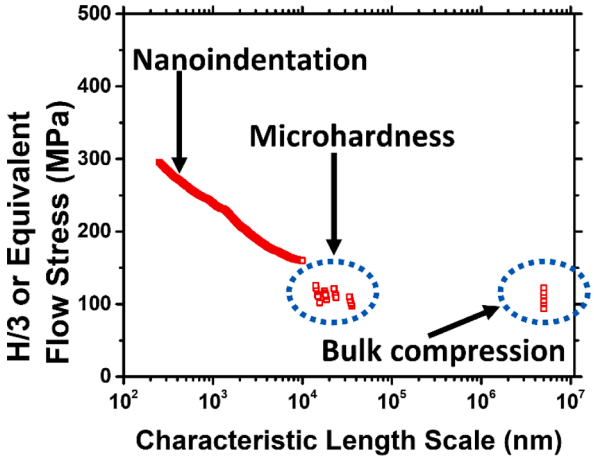

Fig. 5. The flow stress, σ_f, or the hardness divided by 3, (H/3), plotted as a function of a representative length scale. It should be noted that for nanoindentation and microhardness tests, the characteristic length scales are defined by the indentation depths, while for bulk compression tests, the width of the samples is used.

As potential advantages, calcium's relatively high yield strength and its insensitivity to the applied strain rate (i.e., the charging rate) are beneficial in that calcium will likely not significantly creep during operation. More specifically, electrodes are often subjected to static loads during electrochemical cycles, e.g., stack pressures, as well as dynamically varying loads induced by intercalation/de-intercalation or plating/stripping. Electrode materials with low yield strength are prone to deform in undesirable ways (e.g., form surface cracks, suffer large volume changes), which leads to capacity loss and even failure. However, Ca metal's stiff nature may surmount such obstacles in battery systems owing to its higher yield strength (as compared to Li and Na). Furthermore, for intercalation batteries, a concentration gradient of the mobile species often occurs inside the electrode material (in brief, nearby and far from the electrolyte) due to the limited diffusivity, which causes stresses to be generated in the electrode [60–62]. These stresses may cause the electrode to deform irregularly and lose capacity, but calcium may be more resilient to internal stress formation owing to its relatively high strength.

Fig. 2 indicates that Ca metal exhibits a relatively small size effect (hardness varies by a factor of less than two over our large measured range of indentation depths) compared to several other candidates for metallic anodes. For instance, Fincher et al. reported that the hardness of Na metal during room temperature nanoindentation test differs by a factor of ~12 as the indentation depth increased from 250 nm to 10 μm [39]. Also, Fincher at el. found that the hardness of Li varies by a factor of ~6 as the indentation depth increased from 250 nm to 10 μm at room temperature [40]. However, the hardness of Ca metal varies by a factor of only ~1.8 over of a range of depths of 250 nm to 10 μm. This comparatively small size effect may have certain simplifying advantages in modeling, predicting, and thus potentially preventing dendrite growth and other failure mechanisms. For instance, the mechanical behavior of Na and Li dendrites is difficult to model in the sense that their dendrites are relatively hard/strong when they begin to grow at the small (nano) scale, but may become significantly softer/weaker after they grow to a significant size. Several theoretical models have suggested that the strength of the metal itself can significantly affect the dendrite growth process, particularly in all-solid-state-batteries [63–65]. In brief, if the metal deposit has a larger strength, it can place larger stresses on the surrounding materials (e.g., the solid electrolyte). These stresses can lead to the growth of defects in the surrounding materials (e.g., the solid electrolyte), opening a path into which the metal deposit can flow [66,67]. These defective paths can ultimately percolate through the surrounding materials (e.g., solid electrolyte), oftentimes all the way to the cathode, thereby short-circuiting the electrochemical cell. If the strength of the metal itself is unknown or changing as it grows (as is the case in Li and Na metal), it becomes much more difficult to model. By comparison, since we have shown that Ca metal has a relatively small dependence of its properties on the size of the material (here represented by the indentation depth), it will be much more straightforward to model and accurately predict the mechanical response of Ca, e.g., during the formation and growth of a dendrite.

Additionally, we have shown that Ca is relatively insensitive to the applied strain rate. By comparison Li and Na have been shown to be highly sensitive to the applied strain rate. The main source of the discrepancy between the significant strain-rate sensitivity observed in Li and Na and the negligible strain-rate sensitivity observed in Ca stems from the homologous temperature during operation. Since Ca metal has a low homologous temperature at room temperature ($T/T_m = 0.26$ at room temperature), thermally activated processes, such as diffusion and creep-type processes, are relatively limited in calcium, thereby leading to a negligible sensitivity to the applied strain rate. By comparison, Li and Na operate at high homologous temperatures ($T/T_m = 0.65$ for Li and $T/T_m = 0.80$ for Na at room temperature), thus leading to a large sensitivity to the applied strain rate. During battery operation, the charging rate is connected to the strain rate. That is, if the charging rate is high, the battery generally experiences higher strain rates during operation. However, since calcium's mechanical properties are essentially independent of the strain rate, changing the charging rate will not have a direct influence on the strength (and thus stresses generated) in Ca.

Finally, we would like to note that Ca has some desirable properties for potential future applications as a structural battery. A structural battery is a battery that provides the function of both energy storage and mechanical rigidity/support. For example, a mechanically robust battery can be used as a support for building components, car doors, aircraft wings, etc., as well as for energy storage. For such applications, a material that exhibits a relatively high yield strength is required. We have shown that calcium metal is quite strong with a yield strength of 107 ± 4.6 MPa and thus may find potential use as a structural battery. For instance, instead of simply adding batteries to an existing vehicle (thus adding volume/weight), calcium-containing structural batteries could instead replace existing components of the car (e.g., the door), thus reducing the total mass (and volume) of the vehicle.

5. Conclusions

In this study, we have quantified elastic and plastic properties of calcium metal at room temperature using bulk compression tests and nanoindentation. Overall, Ca metal shows a relatively high yield strength of 107 ± 4.6 MPa, is quite insensitive to the applied strain-rate, and exhibits only a small dependence of its mechanical properties on its size (i.e., it does not display a significant "size effect"). Nanoindentation tests also revealed an elastic modulus of ~21.7–25.2 GPa, which is several times larger than that of lithium and sodium metal. Calcium's mechanical response is largely insensitive to the applied strain rate due to its relatively high melting point. As such, calcium will likely not exhibit creep-type deformation during electrochemical operation, and changing the charging rate will likely not have a direct influence the strength (and thus stresses generated) in Ca. Additionally, the relatively limited "size effects" of calcium will render it much more straightforward to model from a mechanical perspective than its alkali metal counterparts (e.g., Li and Na), e.g., in accurately predicting its mechanical response during the formation and growth of a dendrite. Perhaps more importantly, Ca's relatively high yield strength (e.g., compared to Li and Na) may lead to applications as structural batteries that provide both energy storage capabilities as well as mechanical rigidity and support. Overall, we have quantified key mechanical properties of Ca metal from the nano to the bulk scale, which we hope will provide guidance for the design of various battery architectures that remain robust during electrochemical operation.

CRediT authorship contribution statement

Jungho Shin: Conceptualization, Software, Validation, Formal analysis, Investigation, Data curation, Writing – original draft. **Cole D. Fincher:** Conceptualization, Software, Validation, Formal analysis. **Matt Pharr:** Conceptualization, Writing – review & editing, Supervision, Project administration, Funding acquisition.

Declaration of competing interest

The authors declare that they have no known competing financial interests or personal relationships that could have appeared to influence the work reported in this paper.

Data availability

Data will be made available on request.

Acknowledgments

We acknowledge the support of the National Science Foundation, United States under award number DMR-1944674. The authors acknowledge the characterization part of this work was performed in the Texas A & M University Materials Characterization Core Facility (RRID: SCR_022202).

Appendix A. Supplementary data

Supplementary material related to this article can be found online at https://doi.org/10.1016/j.eml.2023.102081.

References

[1] A. Ponrouch, J. Bitenc, R. Dominko, N. Lindahl, P. Johansson, M.R. Palacín, Multivalent rechargeable batteries, Energy Storage Mater. 20 (2019) 253–262.
[2] Y. Liang, H. Dong, D. Aurbach, Y. Yao, Current status and future directions of multivalent metal-ion batteries, Nature Energy 5 (9) (2020) 646–656.
[3] H. Tang, Z. Peng, L. Wu, F. Xiong, C. Pei, Q. An, L. Mai, Vanadium-based cathode materials for rechargeable multivalent batteries: Challenges and opportunities, Electrochem. Energy Rev. 1 (2) (2018) 169–199.
[4] D. Monti, A. Ponrouch, R.B. Araujo, F. Barde, P. Johansson, M.R. Palacín, Multivalent batteries—prospects for high energy density: Ca batteries, Front. Chem. (2019) 79.
[5] R.C. Massé, E. Uchaker, G. Cao, Beyond Li-ion: Electrode materials for sodium-and magnesium-ion batteries, Sci. China Mater. 58 (9) (2015) 715–766.
[6] C. Xu, B. Li, H. Du, F. Kang, Energetic zinc ion chemistry: The rechargeable zinc ion battery, Angew. Chem. 124 (4) (2012) 957–959.
[7] N. Jayaprakash, S. Das, L. Archer, The rechargeable aluminum-ion battery, Chem. Commun. 47 (47) (2011) 12610–12612.
[8] M. Wang, C. Jiang, S. Zhang, X. Song, Y. Tang, H.-M. Cheng, Reversible calcium alloying enables a practical room-temperature rechargeable calcium-ion battery with a high discharge voltage, Nat. Chem. 10 (6) (2018) 667–672.
[9] R.J. Gummow, G. Vamvounis, M.B. Kannan, Y. He, Calcium-ion batteries: Current state-of-the-art and future perspectives, Adv. Mater. 30 (39) (2018), 1801702.
[10] S. Wu, F. Zhang, Y. Tang, A novel calcium-ion battery based on dual-carbon configuration with high working voltage and long cycling life, Adv. Sci. 5 (8) (2018), 1701082.
[11] Y. Zhao, A. Wang, L. Ren, X. Liu, J. Luo, Revealing the solid electrolyte interface on calcium metal anodes, J. Energy Chem. (2022).
[12] H. Song, C. Wang, Current status and challenges of calcium metal batteries, Adv. Energy Sustain. Res. 3 (3) (2022), 2100192.
[13] I.D. Hosein, The promise of calcium batteries: Open perspectives and fair comparisons, ACS Energy Lett. 6 (4) (2021) 1560–1565.
[14] N. Yang, J. Sun, R. Shao, Z. Cao, Z. Zhang, M. Dou, J. Niu, F. Wang, Stable and conductive carbon networks enabling high-performance silicon anodes for lithium-ion batteries, Cell Rep. Phys. Sci. 3 (5) (2022), 100862.
[15] P. Liu, E. Sherman, A. Jacobsen, Design and fabrication of multifunctional structural batteries, J. Power Sources 189 (1) (2009) 646–650.
[16] Y. Jie, Y. Tan, L. Li, Y. Han, S. Xu, Z. Zhao, R. Cao, X. Ren, F. Huang, Z. Lei, Electrolyte solvation manipulation enables unprecedented room-temperature calcium-metal batteries, Angew. Chem., Int. Ed. Engl. 59 (31) (2020) 12689–12693.
[17] M. Pharr, K. Zhao, X. Wang, Z. Suo, J.J. Vlassak, Kinetics of initial lithiation of crystalline silicon electrodes of lithium-ion batteries, Nano Lett. 12 (9) (2012) 5039–5047.
[18] M. Pharr, Z. Suo, J.J. Vlassak, Measurements of the fracture energy of lithiated silicon electrodes of Li-ion batteries, Nano Lett. 13 (11) (2013) 5570–5577.
[19] Y. Zhang, Y. Luo, C. Fincher, S. Banerjee, M. Pharr, Chemo-mechanical degradation in V 2 O 5 thin film cathodes of Li-ion batteries during electrochemical cycling, J. Mater. Chem. A 7 (41) (2019) 23922–23930.
[20] M. Pharr, Y.S. Choi, D. Lee, K.H. Oh, J.J. Vlassak, Measurements of stress and fracture in germanium electrodes of lithium-ion batteries during electrochemical lithiation and delithiation, J. Power Sources 304 (2016) 164–169.

[21] D. Wang, X. Gao, Y. Chen, L. Jin, C. Kuss, P.G. Bruce, Plating and stripping calcium in an organic electrolyte, Nat. Mater. 17 (1) (2018) 16–20.
[22] Z. Zhao-Karger, Y. Xiu, Z. Li, A. Reupert, T. Smok, M. Fichtner, Calcium-tin alloys as anodes for rechargeable non-aqueous calcium-ion batteries at room temperature, Nat. Commun. 13 (1) (2022) 1–9.
[23] J. Bitenc, A. Scafuri, K. Pirnat, M. Lozinšek, I. Jerman, J. Grdadolnik, B. Fraisse, R. Berthelot, L. Stievano, R. Dominko, Electrochemical performance and mechanism of calcium metal-organic battery, Batteries Supercaps 4 (1) (2021) 214–220.
[24] S.D. Pu, C. Gong, X. Gao, Z. Ning, S. Yang, J.-J. Marie, B. Liu, R.A. House, G. O. Hartley, J. Luo, Current-density-dependent electroplating in Ca electrolytes: From globules to dendrites, ACS Energy Lett. 5 (7) (2020) 2283–2290.
[25] B. Ji, H. He, W. Yao, Y. Tang, Recent advances and perspectives on calcium-ion storage: Key materials and devices, Adv. Mater. 33 (2) (2021), 2005501.
[26] Z. Yao, V.I. Hegde, A. Aspuru-Guzik, C. Wolverton, Discovery of calcium-metal alloy anodes for reversible Ca-ion batteries, Adv. Energy Mater. 9 (9) (2019), 1802994.
[27] V. Körstgens, H.-C. Flemming, J. Wingender, W. Borchard, Influence of calcium ions on the mechanical properties of a model biofilm of mucoid pseudomonas aeruginosa, Water Sci. Technol. 43 (6) (2001) 49–57.
[28] B. Zhang, Y. Wang, L. Geng, C. Lu, Effects of calcium on texture and mechanical properties of hot-extruded Mg–Zn–Ca alloys, Mater. Sci. Eng. A 539 (2012) 56–60.
[29] A. Shaw, L. Tian, A.M. Russell, Tensile properties of highpurity Ca metal, British J. Appl. Sci. Technol 15 (6) (2016) 1–6.
[30] W.C. Oliver, G.M. Pharr, An improved technique for determining hardness and elastic modulus using load and displacement sensing indentation experiments, J. Mater. Res. 7 (6) (1992) 1564–1583.
[31] J. Hay, E. Herbert, Measuring the complex modulus of polymers by instrumented indentation testing, Exp. Tech. 37 (2013) 55–61.
[32] J. Hay, P. Agee, E. Herbert, Continuous stiffness measurement during instrumented indentation testing, Exp. Tech. 34 (2010) 86–94.
[33] P.S. Phani, W. Oliver, G. Pharr, Understanding and modeling plasticity error during nanoindentation with continuous stiffness measurement, Mater. Des. 194 (2020), 108923.
[34] B. Merle, V. Maier-Kiener, G.M. Pharr, Influence of modulus-to-hardness ratio and harmonic parameters on continuous stiffness measurement during nanoindentation, Acta Mater. 134 (2017) 167–176.
[35] A. Shaw, L. Tian, A. Russell, Tensile properties of high-purity Ca metal, 2016.
[36] C.A. Hampel, M. Kolodney, Rare metals handbook, J. Electrochem. Soc. 108 (11) (1961) 248C.
[37] Mechanical properties of calcium, 2015 https://metals.comparenature.com /en/mechanical-properties-of-calcium/model-12-3.
[38] Calcium (Ca) - Properties, Applications, 2013 https://www.azom.com/article. aspx?ArticleID=9098.
[39] C.D. Fincher, Y. Zhang, G.M. Pharr, M. Pharr, Elastic and plastic characteristics of sodium metal, ACS Appl. Energy Mater. 3 (2) (2020) 1759–1767.
[40] C.D. Fincher, D. Ojeda, Y. Zhang, G.M. Pharr, M. Pharr, Mechanical properties of metallic lithium: From nano to bulk scales, Acta Mater. 186 (2020) 215–222.
[41] A. Everts, G. Bagley, Physical and electrical properties of calcium, J. Electrochem. Soc. 93 (6) (1948) 265.
[42] M.E. Kassner, New developments in understanding Harper–Dorn, five-power law creep and power-law breakdown, Metals 10 (10) (2020) 1284.
[43] J. Weertman, Theory of steady-state creep based on dislocation climb, J. Appl. Phys. 26 (10) (1955) 1213–1217.
[44] T.H. Courtney, Mechanical Behavior of Materials, Waveland Press, 2005.
[45] K.C. Le, Two universal laws for plastic flows and the consistent thermodynamic dislocation theory, Mech. Res. Commun. 109 (2020), 103597.
[46] E. ToolBox, Engineering ToolBox, (2008), 2008. Metals - Strength vs. Temperature. [online] Available at: https://www.engineeringtoolbox.com/metal-temperature-strength-d_1353.html.
[47] A. Argon, Strengthening Mechanisms in Crystal Plasticity, OUP Oxford, 2007.
[48] C.M. Byer, K. Ramesh, Effects of the initial dislocation density on size effects in single-crystal magnesium, Acta Mater. 61 (10) (2013) 3808–3818.
[49] D. Tabor, The Hardness of Metals, Oxford University Press, 2000.
[50] A. Palenzona, P. Manfrinetti, M. Fornasini, Phase diagram of the Ca–Sn system, J. Alloys Compd. 312 (1–2) (2000) 165–171.
[51] H. Okamoto, Ca-Zn (calcium-zinc), J. Phase Equilibria Diffusion 34 (2) (2013) 171.
[52] P. Franke, D. Neuschütz, Binary systems. Part 5: Binary systems supplement 1, 2007.
[53] X. Xu, M. Duan, Y. Yue, Q. Li, X. Zhang, L. Wu, P. Wu, B. Song, L. Mai, Bilayered Mg0, 25V2O5 · H2O as a stable cathode for rechargeable Ca-ion batteries, ACS Energy Lett. 4 (6) (2019) 1328–1335.
[54] Z.-L. Xu, J. Park, J. Wang, H. Moon, G. Yoon, J. Lim, Y.-J. Ko, S.-P. Cho, S.-Y. Lee, K. Kang, A new high-voltage calcium intercalation host for ultra-stable and high-power calcium rechargeable batteries, Nat. Commun. 12 (1) (2021) 1–9.
[55] P. Barai, K. Higa, V. Srinivasan, Effect of initial state of lithium on the propensity for dendrite formation: A theoretical study, J. Electrochem. Soc. 164 (2) (2016) A180.
[56] T. Krauskopf, H. Hartmann, W.G. Zeier, J.r. Janek, Toward a fundamental understanding of the lithium metal anode in solid-state batteries—An electrochemo-mechanical study on the garnet-type solid electrolyte Li6, 25Al0. 25La3Zr2O12, ACS Appl. Mater. Interfaces 11 (15) (2019) 14463–14477.
[57] M.J. Wang, R. Choudhury, J. Sakamoto, Characterizing the Li-solid-electrolyte interface dynamics as a function of stack pressure and current density, Joule 3 (9) (2019) 2165–2178.
[58] X. Yin, W. Tang, K.C. Phua, S. Adams, S.W. Lee, G.W. Zheng, Insights into morphological evolution and cycling behaviour of lithium metal anode under mechanical pressure, Nano Energy 50 (2018) 659–664.
[59] J. Shin, M. Pharr, Fracture behavior of metallic sodium and implications for battery applications, Mater. Horiz. (2022).
[60] J.-H. Park, Y.-S. Choi, Y.-W. Byeon, J.-P. Ahn, J.-C. Lee, Diffusion kinetics governing the diffusivity and diffusion anisotropy of alloying anodes in na-ion batteries, Nano Energy 65 (2019), 104041.
[61] Y.W. Byeon, J.P. Ahn, J.C. Lee, Diffusion along dislocations mitigates self-limiting Na diffusion in crystalline Sn, Small 16 (52) (2020), 2004868.
[62] Y.S. Choi, D.O. Scanlon, J.C. Lee, Extending the performance limit of anodes: insights from diffusion kinetics of alloying anodes, Adv. Energy Mater. 11 (27) (2021), 2003078.
[63] C. Monroe, J. Newman, Dendrite growth in lithium/polymer systems: A propagation model for liquid electrolytes under galvanostatic conditions, J. Electrochem. Soc. 150 (10) (2003) A1377.
[64] C. Monroe, J. Newman, The impact of elastic deformation on deposition kinetics at lithium/polymer interfaces, J. Electrochem. Soc. 152 (2) (2005) A396.
[65] P. Barai, K. Higa, V. Srinivasan, Lithium dendrite growth mechanisms in polymer electrolytes and prevention strategies, Phys. Chem. Chem. Phys. 19 (31) (2017) 20493–20505.
[66] L. Porz, T. Swamy, B.W. Sheldon, D. Rettenwander, T. Frömling, H.L. Thaman, S. Berendts, R. Uecker, W.C. Carter, Y.M. Chiang, Mechanism of lithium metal penetration through inorganic solid electrolytes, Adv. Energy Mater. 7 (20) (2017), 1701003.
[67] F. Han, A.S. Westover, J. Yue, X. Fan, F. Wang, M. Chi, D.N. Leonard, N.J. Dudney, H. Wang, C. Wang, High electronic conductivity as the origin of lithium dendrite formation within solid electrolytes, Nat. Energy 4 (3) (2019) 187–196.